Reduced Derivatives of the Mn Cluster in the Oxygen-Evolving Complex of Photosystem II: An EXAFS Study

Pamela J. Riggs-Gelasco,[†] Rui Mei,[‡,§] Charles F. Yocum,*[,†,‡] and James E. Penner-Hahn*[,†]

Contribution from the Departments of Chemistry and Biology, University of Michigan, 930 North University Avenue, Ann Arbor, Michigan 48109-1055

Received February 9, 1995. Revised Manuscript Received October 16, 1995[⊗]

Abstract: X-ray absorption spectroscopy (XAS) has been used to characterize the local structural environment of the Mn in the resting (S_1) state and two different reduced derivatives of the photosynthetic oxygen-evolving complex (OEC). Short-term incubation with NH_2OH gives a state with minimal structural rearrangement relative to the S_1 state, consistent with the small shift in X-ray absorption edge energy for the NH_2OH reduced sample. In contrast, hydroquinone reduced samples show significant structural rearrangements, including the appearance of a new Mn−O shell at 2.17 Å and a decrease in the amplitude of the 2.7 Å Mn···Mn interaction. These changes are consistent with hydroquinone producing a reduced state consisting of ca. 2 Mn(II) and a single, oxidized $Mn_2(\mu\text{-}O)_2$ core. The interaction assigned to Mn···Mn or Mn···Ca scattering at ca. 3.3 Å is not present in the hydroquinone reduced sample, but is present in the EXAFS of the NH_2OH reduced sample. The effects of both NH_2OH and hydroquinone are reversed by illumination and dark adaptation, indicating that the reductant induced changes are not the result of sample decomposition. Long-term incubation with NH_2OH and short-term incubation with higher concentrations of NH_2OH both result in greater reduction, more extensive structural change, and loss of activity. There is a linear correlation between the activity of these highly reduced samples and the Mn content of the samples. However, the activity per Mn atom remains constant, demonstrating that all of the Mn detected by XAS is present in active OEC centers. This demonstrates that highly reduced centers can be produced not only by hydroquinone but also by NH_2-OH. However, when NH_2OH is used to produce highly reduced centers, Mn loss competes with reduction. Based on differences in the reactivity of these reduced states and on their very different structural properties, a refined mechanism for reduction of Mn in the OEC is proposed.

The Oxygen-Evolving Complex (OEC)[1] of Photosystem II (PSII) catalyzes the 4-electron oxidation of two water molecules to dioxygen (eq 1). This reaction is the source of most of the

$$2H_2O \rightarrow O_2 + 4H^+ + 4e^- \qquad (1)$$

molecular oxygen in the atmosphere and provides the reducing equivalents needed for reduction of CO_2 to glucose. Although substantial progress has been made in resolving the structure and function of PSII, the detailed mechanism of water oxidation is not well understood. Isolated PSII consists of a complex of several different polypeptides; some bind chlorophyll and others serve to arrange structurally the inorganic cofactors required for oxygen evolution (4 Mn ions, Cl^-, and Ca^{2+}).[2−4] Water oxidation begins with the photoexcitation of a specialized chlorophyll complex (P_{680}), whose photooxidation triggers a chain of electron transfer events resulting in the reduction of plastoquinone on the electron acceptor side of PS II. $P_{680}{}^+$ is re-reduced by the electron donor side of PSII, consisting of a redox active tyrosine residue[5] and the Mn cluster of the OEC. Sequential oxidation of the Mn cluster by $P_{680}{}^+$ generates the four oxidizing equivalents required by eq 1. The OEC then catalyzes the four-electron oxidation of two water molecules.

A major advance in the understanding of the mechanism of water oxidation was the observation that oxygen release from PSII shows a periodicity of 4 when exposed to short flashes of light.[6] Kok first proposed that the OEC cycles through several intermediates, labeled S states.[7,8] In the S_i nomenclature, the subscript represents the number of oxidizing equivalents that have been stored. Since S_0 is slowly oxidized to S_1,[9] and S_2 and S_3 decay rapidly ($t_{1/2}$ = 60−90 s) to S_1, dark adaptation gives a population of PSII in which S_1 predominates.[10−12] Following formation of S_4, the OEC is reduced to S_0 with the concomitant oxidation of water (see Scheme 1).

* Authors to whom correspondences should be addressed.
† Department of Chemistry, University of Michigan.
‡ Department of Biology, University of Michigan.
§ Present address: Department of Biochemistry, Stanford University, Beckman Center, Stanford, CA 94305.
⊗ Abstract published in *Advance ACS Abstracts,* February 15, 1996.

(1) Abbreviations used: chl = chlorophyll; EDTA = ethylenedamine-tetraacetic acid; EPR = electron paramagnetic resonance; EXAFS = Extended X-ray Absorption Fine Structure; HB(3,5-iPr$_2$pz)$_3$ = hydrotris-(3,5-diisopropyl-1-pyrazolyl)borate; kDa = kilodalton; MES = 2-(*N*-morpholino)ethanesulfonic acid; OEC = Oxygen Evolving Complex; PSII = Photosystem II; salpn = 1,3-bis(salicylideneiminato)propane; tphpn = *N,N,N′,N′*-tetrakis(2-pyridylmethyl)-2-hydroxypropane-1,3-diamine; UV = ultraviolet; XANES = X-ray Absorption Near Edge Structure; XAS = X-ray Absorption Spectrscopy.

(2) Sivaraja, M.; Dismukes, G. C. *Biochemistry* **1988**, *27*, 3467−3475.
(3) Cheniae, G.; Martin, I. *Biochim. Biophys. Acta* **1970**, *197*, 219−239.
(4) Yocum, C. F.; Yerkes, C. T.; Blankenship, R. E.; Sharp, R. R.; Babcock, G. T. *Proc. Natl. Acad. Sci. U.S.A.* **1981**, *78*, 7507−7511.
(5) Hoganson, C. W.; Babcock, G. T. *Biochemistry* **1988**, *27*, 5848−5855.
(6) Joliet, P.; Barbierri, G.; Chabaud, R. *Photochem. Photobiol.* **1969**, *10*, 309−329.
(7) Kok, B.; Forbush, B.; McGloin, M. *Photochem. Photobiol.* **1970**, *11*, 457.
(8) Forbush, B.; Kok, B.; McGloin, M. P. *Biochim. Biophys. Acta* **1971**, *14*, 307−321.
(9) Styring, S.; Rutherford, A. W. *Biochemistry* **1987**, *26*, 2401−2405.
(10) Vermass, W. F. J.; Renger, G.; Dohnt, G. *Biochim. Biophys. Acta* **1984**, *764*, 194−202.
(11) Velthuys, B. R.; Visser, J. W. M. *FEBS Lett.* **1975**, *55*, 109−112.
(12) Babcock, G. T.; Sauer, K. *Biochim. Biophys. Acta* **1973**, *325*, 483−503.

Scheme 1

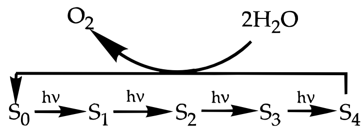

S-state advancements are believed to involve Mn oxidation in $S_0 \rightarrow S_1$, $S_1 \rightarrow S_2$, and possibly $S_2 \rightarrow S_3$.[13] Absorption changes in the ultraviolet, attributed to Mn−ligand charge transfer transitions, occur with a periodicity of four.[14] In addition, a Mn-associated multiline EPR signal is uniquely associated with the S_2 state.[15−17] Centered at $g \approx 2$, this signal consists of 16−20 hyperfine lines and is proposed to arise from a mixed-valence Mn cluster.[18−21] A broad signal at $g \approx 4$ can be obtained in place of the $g \approx 2$ multiline signal by use of appropriate cryoprotectants or by manipulating inorganic ion cofactors.[22] The $g \approx 4$ signal also derives from a multinuclear Mn cluster, as demonstrated by the presence of hyperfine structure in ammonia-treated, oriented samples.[23,24] The stable S_1 state lacks conventional EPR signals. However, an integer spin EPR signal was detected for S_1 using parallel mode EPR.[25] The signal disappears proportionately with the formation of S_2, leading to the conclusion that the species giving rise to the parallel spin signal is a precursor form of the multinuclear cluster giving rise to the multiline signal.

X-ray absorption spectroscopy (XAS) has proven to be an important spectroscopic tool in the structural characterization of the Mn cluster. Extended X-ray absorption fine structure (EXAFS) spectra can be analyzed to give nearest neighbor bond lengths with an accuracy of ca. 0.02 Å and coordination numbers with an uncertainty of ±25%.[26−28] X-ray absorption near edge structure (XANES) spectra yield information about the metal site geometry and oxidation state. Early EXAFS investigations established that the Mn coordination sphere consists predominantly of oxygen and/or nitrogen ligands.[29−31] In addition, the cluster contains one or more di-μ-oxo bridged Mn dimers, based on the observation of 2.7 Å Mn···Mn vectors. With advances in detector and sample quality, an additional metal−metal interaction at 3.3 Å was subsequently reported.[32−34]

Early XANES studies supported the proposal that the Mn cluster was indeed the site for storage of oxidizing equivalents. The XANES energy for S_1 suggests that the average Mn oxidation state is greater than 3 and less than 4.[34−36] The presence of di-μ-oxo bridged Mn also points to oxidation states ≥ 3.[37−39] The X-ray absorption edge energy increases when S_1 is oxidized to S_2, confirming that Mn is oxidized. Comparable edge shifts are observed for both the multiline form and the $g \approx 4$ form of S_2, suggesting that the EPR differences are due to conformational rather than oxidation state differences.[40,41] Early reports showed no change in XANES energy for the $S_2 \rightarrow S_3$ transition,[41,42] consistent with EPR evidence that a protein residue can be oxidized on the $S_2 \rightarrow S_3$ transition.[43−46] More recently, Ono et al. have reported XANES evidence that Mn oxidation occurs not only for the $S_1 \rightarrow S_2$ transition but also for the $S_2 \rightarrow S_3$ and $S_0 \rightarrow S_1$ transitions.[36] This suggests that Mn, rather than a protein residue, may be oxidized with these S state transitions. UV−visible absorption changes support Mn-centered oxidations as well; however, this question remains controversial.[47]

In this study, we have employed two reductants, NH_2OH and hydroquinone (H_2Q), in order to provide additional spectroscopic and mechanistic insight into the enzymatic cycle of the OEC. For many years, NH_2OH has been employed as a substrate analogue for H_2O and it has been noted that low concentrations of NH_2OH[48] (as well as NH_2NH_2[49−51] and H_2O_2[52,53]) delay the normal flash-dependent release of oxygen by two flashes. A two-flash delay has also been observed in formation of the

(13) Debus, R. J. *Biochim. Biophys. Acta* **1992**, *1102*, 269−352.
(14) Pulles, M. P. J.; Van Gorkhom, H. J.; Willemsen, J. G. *Biochim. Biophys. Acta* **1976**, *461*, 167−181.
(15) Dismukes, G.; Siderer, Y. *FEBS Lett.* **1980**, *121*, 78−80.
(16) Dismukes, G. C.; Siderer, Y. *Proc. Natl. Acad. Sci. U.S.A.* **1981**, *78*, 274−278.
(17) Brudvig, G. W.; Casey, J. L.; Sauer, K. *Biochim. Biophys. Acta* **1983**, *723*, 366−371.
(18) de Paula, J. C.; Beck, W. F.; Brudwig, G. W. *J. Am. Chem. Soc.* **1986**, *108*, 4002−4009.
(19) Haddy, A.; Aasa, R.; Andreasson, L.-E. *Biochemistry* **1989**, *28*, 6954−6959.
(20) Britt, R. D.; Lorigan, G. A.; Sauer, K.; Klein, M. P.; Zimmerman, J.-L. *Biochim. Biophys. Acta* **1992**, *1040*, 95−101.
(21) Kusunoki, M. *Chem. Phys. Lett.* **1992**, *197*, 108−116.
(22) Casey, J.; Sauer, K. *Biochim. Biophys. Acta* **1984**, *767*, 21−28.
(23) Kim, D. H.; Britt, R. D.; Klein, M. P.; Sauer, K. *J. Am. Chem. Soc.* **1990**, *112*, 9389−91.
(24) Kim, D. H.; Britt, R. D.; Klein, M. P.; Sauer, K. *Biochemistry* **1992**, *31*, 541−7.
(25) Dexheimer, S. L.; Klein, M. P. *J. Am. Chem. Soc.* **1992**, *114*, 2821−2826.
(26) Scott, R. *Methods Enzymol.* **1985**, *117*, 414−459.
(27) Penner-Hahn, J. E. In *Metal Clusters in Proteins*; Que, L., Ed.; American Chemical Society: Washington, DC, 1988; Vol. 372, pp 28-48.
(28) Fay, M. J.; Proctor, A.; Hoffmann, D. P.; Hercules, D. M. *Anal. Chem.* **1988**, *60*, 1225A-1243A.
(29) Yachandra, V. K.; Guiles, R. D.; McDermott, A.; Britt, R. D.; Dexheimer, S. L.; Sauer, K.; Klein, M. P. *Biochim. Biophys. Acta* **1986**, *850*, 324−332.
(30) Yachandra, V. K.; Guiles, R. D.; McDermott, A. E.; Cole, J. L.; Britt, R. D.; Dexheimer, S. L.; Sauer, K.; Klein, M. P. *Biochemistry* **1987**, *26*, 5974−5981.
(31) Guiles, R. D.; Yachandra, V. K.; McDermott, A. E.; Britt, R. D.; Dexheimer, S. L.; Sauer, K.; Klein, M. P. In *Progress in Photosynthesis Research*; Biggens, J., Ed.; Martinus Nijhoff Publishers: Dordrecht, The Netherlands, 1987; Vol. 1, pp 1.5.561−1.5.564.
(32) Penner-Hahn, J. E.; Fronko, R. H.; Pecoraro, V. L.; Yocum, C. F.; Betts, S. D.; Bowlby, N. R. *J. Am. Chem. Soc.* **1990**, *112*, 2549−2557.
(33) George, G. N.; Prince, R. C.; Cramer, S. P. *Science* **1989**, *243*, 789−791.
(34) Yachandra, V. K.; DeRose, V. J.; Latimer, M. J.; Mukerji, I.; Sauer, K.; Klein, M. P. *Science* **1993**, *260*, 675−679.
(35) Riggs, P. J.; Mei, R.; Yocum, C. F.; Penner-Hahn, J. E. *J. Am. Chem. Soc.* **1992**, *114*, 10650−51.
(36) Ono, T.-a.; Noguchi, T.; Inoue, Y.; Kusunoki, M.; Matsushita, T.; Oyanagi, H. *Science* **1992**, *258*, 1335−1337.
(37) Goodson, P. A.; Oki, A. R.; Glerup, J.; Hodgson, D. J. *J. Am. Chem. Soc.* **1990**, *112*, 6248−6254.
(38) Goodson, P. A.; Hodgson, D. J. *Inorg. Chem.* **1989**, *28*, 3606−3608.
(39) Kitajima, N.; Sihgh, U. P.; Amagai, H.; Osawa, M.; Moro-oka, Y. *J. Am. Chem. Soc.* **1991**, *113*, 7757−7758.
(40) Cole, J.; Yachandra, V. K.; Guiles, R. D.; McDermott, A. E.; Britt, R. D.; Dexheimer, S. L.; Sauer, K.; Klein, M. P. *Biochim. Biophys. Acta* **1987**, *890*, 395−398.
(41) Goodin, D. B.; Yachandra, V. K.; Britt, R. D.; Sauer, K.; Klein, M. *Biochim. Biophys. Acta* **1984**, *767*, 209−216.
(42) Guiles, R. D.; J.-L., Z.; McDermott, A. E.; Yachandra, V. K.; Cole, J. L.; Dexheimer, S. L.; Britt, R. D.; Wieghardt, K.; Bossek, U.; Sauer, K.; Klein, M. P. *Biochemistry* **1990**, *29*, 471−485.
(43) Boussac, A.; Zimmerman, J.-L.; Rutherford, A. W. *Biochemistry* **1989**, *28*, 8984−8989.
(44) Boussac, A.; Zimmerman, J.-L.; Rutherford, A. W. *FEBS Lett.* **1990**, *277*, 69−74.
(45) Boussac, A.; Zimmerman, J.-L.; Rutherford, A. W. In *Current Research in Photosynthesis*; Baltscheffsky, M., Ed.; Kluwer Academic Publishers: The Netherlands, 1990; Vol. 1, pp 713−716.
(46) Ono, T.-a.; Inoue, Y. *Biochemistry* **1991**, *30*, 6183−6188.
(47) Dekker, J. P. In *Manganese Redox Enzymes*; Pecoraro, V. L., Ed.; VCH Publishers: New York, 1992; pp 85−104.
(48) Bouges, B. *Biochim. Biophys. Acta* **1971**, *234*, 103−112.
(49) Hanssum, B.; Renger, G. *Biochim. Biophys. Acta* **1985**, *810*, 225−234.
(50) Radmer, R. *Biochim. Biophys. Acta* **1981**, *637*, 80−87.
(51) Renger, G.; Bader, K. P.; Schmid, G. H. *Biochim. Biophys. Acta* **1990**, *1015*, 288−294.
(52) Mano, J.; Takahashi, M.-a.; Asada, K. *Biochemistry* **1987**, *26*, 2495−2501.
(53) Velthuys, B.; Kok, B. *Biochim. Biophys. Acta* **1978**, *502*, 211−221.

S_2 multiline signal,[2,54] in the proton release patterns,[55] and in quaternary oscillations in absorption changes.[56] Two explanations for the delay have been proposed: (1) A two-electron reduction of the Mn cluster by NH_2OH to form an "S_{-1}" state[52−54,57−62] or (2) formation of a stable S_1·NH_2OH complex where the bound NH_2OH serves to reduce a higher S state (e.g., S_2) following photooxidation.[34,50,63,64]

Model 1 is supported by the fact that the delay in oxygen evolution persists even after removal of NH_2OH and long-term dark incubation.[61] Recently, we have reported that the X-ray absorption edge shifts to lower energy after NH_2OH incubation, consistent with the reduction of Mn in the dark.[35] This edge shift is completely reversed by continuous illumination, demonstrating that the Mn reduction is not an artifact of inactive centers. In contrast, Guiles et al. did *not* observe a XANES edge shift following incubation with low concentrations of NH_2OH, but did observe a decrease in edge energy after a single flash.[63] This was interpreted as evidence of a stable, NH_2OH-bound intermediate (model 2). Nitrogen release has been observed when NH_2OH treated PSII is treated with one flash of light.[50,64] This observation appears to support model 2, with photooxidation of bound NH_2OH. However, it has been argued that the N_2 yield was too low, relative to the measured O_2 yield, to support the binding of NH_2OH in the dark[56] and that the observed N_2 production could take place at Mn-depleted centers.[54]

In addition to stable S_{-1} state(s), evidence has recently been presented that a stable S_{-2} state can be produced by hydrazine[57−59,62] or hydroxylamine treatments.[58,59,62] Also, high concentrations of reductants are known to cause irreversible release of Mn(II).[4,65−67] It has been proposed that the release of Mn(II) is associated with the formation of a labile, unstable S_{-3} state.[60,67,68] Reduced derivatives such as S_{-2} and S_{-3} may be intermediates in the process of photoactivation, in which active, oxidized centers are generated by illuminating Mn-depleted PSII supplemented with Mn(II), Ca(II), and Cl^-.[69−73] As S_1 is thought to contain only Mn(III) and Mn(IV), reduced states of the OEC must necessarily exist below S_0 in order to explain the photoactivation process.

In addition to NH_2OH, we have employed larger reductants, such as hydroquinone (H_2Q), to probe active site access and Mn reduction. In preparations devoid of the 17 and 23 kDa extrinsic polypeptides, both NH_2OH and hydroquinone inhibition can be substantially delayed by the presence of Ca^{2+}.[68] Hydroquinone reduction is slower (tens of minutes) than NH_2OH reduction (minutes) but results in the formation of a species with a Mn(II) six-line EPR signal.[67] This Mn(II) is not EDTA extractable and does not cause enhancement of the solvent ^1H-NMR relaxation, leading to the conclusion that the Mn(II) produced by hydroquinone is sequestered near its active site.[67] We have previously reported that hydroquinone treatment leads to a significant decrease in XANES edge energy.[35] We find, from analysis of both EPR[67] and XANES[35] spectra, that roughly 50% of the OEC Mn is reduced to Mn(II) following hydroquinone treatment. As with NH_2OH treatment, this reduction is completely photoreversible as judged by activity, disappearance of the 6-line EPR signal, and the return of the XANES edge position to that of the control.

In this paper, we present the structural characterization of hydroquinone and hydroxylamine reduced PSII samples using EXAFS spectroscopy. Structural comparisons of these two reduced species provide new insight into the mechanism of the OEC.

Experimental Section

Sample Preparation. PSII enriched membranes[74] were treated with octylglucopyranoside in a high ionic strength buffer according to the method of Ghanotakis et al.[75] This preparation, referred to as the "reaction center complex", is devoid of the 23 and 17 kDa extrinsic polypeptides and the light harvesting complex (LHC), a collection of antenna chlorophyll binding proteins. This highly purified preparation was used for all XAS measurements because of its relatively high Mn concentration. A standard Clark-type oxygen electrode was used to assay enzymatic activity. The assays were conducted in a 50 mM MES (pH 6) buffer containing 10 mM $CaCl_2$; 0.31 mM 2,6-dichlorobenzoquinone was used as an acceptor. Typical rates for control samples (dark adapted S_1 poised centers) were in the range of 1100−1400 μmol of O_2/mg of chlorophyll/h.

Reduction of PSII samples with 100 μM NH_2OH was carried out for 3 min; the reaction was stopped by a 40-fold dilution in 50 mM MES (pH 6) containing 10 mM $CaCl_2$. Reduction with 200 μM hydroquinone was carried out for 30 min. In some studies, $K_3Fe(CN)_6$ was employed to terminate the H_2Q reduction reaction (final concentration of 500 μM). In other studies, the reaction was slowed by removing the excess H_2Q by centrifugation. The chlorophyll concentration during both incubations was 0.67 mg/mL; all incubations were conducted in the dark. In some experiments, aliquots of treated samples were diluted to 0.05 mg/mL and illuminated with room light for 3 min while on ice. Samples were dark adapted after illumination to regenerate the S_1 state. All XAS samples were centrifuged at 40000*g* (6 min) to remove as much H_2O as possible from the remaining pellet. The Mn concentration in such pellets is estimated to be 1.5 mM.[32] Samples were loaded into lucite cuvettes and were stored in the dark at 77 K. The front face of each sample was covered with 6 μm X-ray polypropylene film (Chemplex Industries). Sensitivity to EDTA was confirmed for NH_2OH reduced samples as previously reported.[67]

Measurements. X-ray absorption measurements were made at 10 K using an Oxford Instruments liquid He flow cryostat. EXAFS data were measured either at the Stanford Synchrotron Radiation Laboratory (SSRL) beamline 7−3 or at the National Synchrotron Light Source (NSLS) beamline X19A using a Si(220) (at SSRL) or Si(111) (at NSLS) double crystal monochromator. NH_2OH titration data were collected at NSLS beamline X19A with Si(111) crystals. Harmonic rejection was achieved by detuning the incident intensity by 50%. Both beamlines were equipped with a Canberra 13-element solid state Ge

(54) Beck, W. F.; Brudvig, G. W. *Biochemistry* **1987**, *26*, 8285−8295.
(55) Förster, V.; Junge, W. In *Progress in Photosynthesis Research*; Martinus Nijhoff Publishers: 1987; pp 511−514.
(56) Saygin, O.; Witt, H. T. *Photobiochem. Photobiophys.* **1985**, *10*, 71−82.
(57) Messinger, J., Renger, G. *Biochemistry* **1993**, *32*, 9379−9386.
(58) Kretschmann, H.; Witt, H. T. *Biochim. Biophys. Acta* **1993**, *1144*, 331−345.
(59) Messinger, J., Pauly, S., Witt, H. T. *Z. Naturforsch* **1991**, *46C*, 1033−1038.
(60) Beck, W. F.; Brudvig, G. W. *J. Am. Chem. Soc.* **1988**, *110*, 1517−23.
(61) Kretschmann, H.; Pauly, S.; Witt, H. T. *Biochim. Biophys. Acta* **1991**, *1059*, 208−14.
(62) Messinger, J.; Wacker, U.; Renger, G. *Biochemistry* **1991**, *30*, 7852−7862.
(63) Guiles, R. D.; Yachandra, V. K.; McDermott, A. E.; Cole, J. L.; Dexheimer, S. L.; Britt, R. D.; Sauer, K.; Klein, M. P. *Biochemistry* **1990**, *29*, 486−496.
(64) Radmer, R.; Ollinger, O. *FEBS Lett.* **1982**, *144*, 162−166.
(65) Ghanotakis, D. F.; Topper, J. N.; Yocum, C. F. *Biochim. Biophys. Acta* **1984**, *767*, 524−531.
(66) Cheniae, G. M.; Martin, I. F. *Plant Physiol.* **1971**, *47*, 568−575.
(67) Mei, R.; Yocum, C. F. *Biochemistry* **1992**, *31*, 8449−8454.
(68) Mei, R.; Yocum, C. F. *Biochemistry* **1991**, *30*, 7836−7842.
(69) Miyao, M.; Inoue, Y. *Biochim. Biophys. Acta* **1991**, *1056*, 47−56.
(70) Tamura, N.; Cheniae, G. *Biochim. Biophys. Acta* **1987**, *890*, 179−94.
(71) Tamura, N.; Inoue, Y.; Cheniae, G. M. *Biochim. Biophys. Acta* **1989**, *976*, 173−181.
(72) Miller, A. F.; Brudvig, G. W. *Biochemistry* **1989**, *28*, 8181−90.
(73) Miller, A.-F.; Brudvig, G. W. *Biochemistry* **1990**, *29*, 1385−1392.
(74) Berthold, D. A.; Babcock, G. T.; Yocum, C. F. *FEBS Lett.* **1981**, *134*, 231−234.
(75) Ghanotakis, D. F.; Demetriou, D. M.; Yocum, C. F. *Biochim. Biophys. Acta* **1987**, *891*, 15−21.

detector for monitoring the Mn Kα fluorescence. Spectra were calibrated by simultaneously measuring the absorption spectrum of $KMnO_4$; the distinctive $KMnO_4$ pre-edge feature was assigned a value of 6543.3 eV. All spectra discussed in this paper were reproduced at least once with separate samples. Scans were typically defined with a 5 eV spacing in the pre-edge region (6300−6530 eV, 1 s/point), a 0.25 eV spacing in the edge region (6530−6565 eV; 2 s/point), and 0.05 Å^{-1} spacing in the EXAFS region (1.6−11.9 Å^{-1}, k^3 weighted data collection time). Reported EXAFS spectra are the average of 12−18 45-min scans and represent approximately 4×10^6 useful fluorescence counts/spectrum at k =11.9 Å^{-1} (≈20 s/point × 16 scans/spectra × 1000 fluorescence counts/s × 13 channels/scan). The total incident count rate (ICR) was constrained to be <40 000 counts/s to minimize detector deadtime distortions in the data. Deadtime calibration scans were generated by collecting 200 points at constant energy (7000 eV) over two decades of I_0 intensities. To correct for detector deadtime response, windowed fluorescence counts (FF) were plotted against ICR for each channel. The resulting curve was fit using a least-squares method to a paralyzable deadtime model.[76−78] Typical values were 4.5−6 μs, depending on channel and sample concentration. For the reduced samples and the corresponding controls, the count rates used were within the linear portion of the FF vs ICR curve.

Data Analysis. The EXAFS, $\chi(E)$, is defined as the fractional modulation of the X-ray absorption coefficient:

$$\chi(E) = \frac{\mu(E) - \mu_0(E)}{\mu_0(E)} \approx \frac{\mu(E) - \mu_s(E)}{\mu_f(E)} \tag{2}$$

where $\mu(E)$ is the observed absorption cross section and $\mu_0(E)$ is the cross section in the absence of any EXAFS effects. μ_0 is approximated by μ_s, a smooth polynomial spline that is fit through the observed EXAFS oscillations. The difference between the observed EXAFS and the spline is then ratioed to μ_f, the expected theoretical falloff of the cross section with energy. μ_s was calculated using either 2 or 3 region cubic splines; regions were chosen to minimize the low R background as judged by the resulting Fourier transform.

When converted from a function of energy to a function of k, the photoelectron wave vector, the EXAFS can be written:

$$\chi(k) = \sum \frac{N_s A_s(k) S}{k R_{as}^2} \exp(-2k^2\sigma_{as}^2) \times \exp(-2R_{as}/\lambda)\cdot\sin(2kR_{as} + \phi_{as}(k)) \tag{3}$$

where $k = (2m_e(E - E_0)/\hbar^2)^{1/2}$. E_0 is the threshold energy for the excitation of a core electron and m_e is the mass of the electron. In initial calculations, E_0 was defined as 6555 eV. The variables in the EXAFS equation (eq 3) are defined as follows: N_s is the number of scattering atoms for a given shell; σ_{as} is the mean-square deviation in R_{as}, the absorber−scatterer distance; λ is the mean-free path of the photoelectron; $\phi_{as}(k)$ is the phase shift that the photoelectron undergoes as it passes through the potentials of the absorbing and scattering atoms; and $A_s(k)$ is the back-scattering amplitude function. Thus eq 3 is a sum over all absorber−scatterer pairs. Two additional parameters that are often treated as variables are ΔE_0 and the scale factor, S. ΔE_0 arises from the ambiguous definition of E_0, the energy at which the photoelectron is initially ejected. ΔE_0 and distance show a negative correlation, with an increase of ≈0.01 Å in bond length for every 2−3 eV decrease in ΔE_0. The need for a scale factor arises when using theoretical EXAFS amplitude functions because the theoretical amplitudes typically overestimate the real amplitude functions. The appropriate scale factor was chosen by fixing the coordination number of a structurally characterized compound to the proper value and allowing the scale factor to refine.

The Fourier transform of the EXAFS gives a pseudoradial distribution function, with the peaks shifted by ∼0.4 Å to lower R due to the $\phi_{as}(k)$ term in eq (3). Fourier filtering allows the EXAFS due to each major peak to be isolated, thus simplifying the fitting of eq (3). The danger with Fourier filtering is that it can perturb the EXAFS spectra by introducing truncation effects.[79] For this reason, only wide filters were used (over the three major FT peaks) and all filtered fits discussed in this paper were confirmed with fits to the unfiltered data. Because OEC samples contain endogenous Fe (Fe K edge ≈ 7100 eV), the upper limit to the data was 11.9 Å^{-1}. Fourier transforms and curve fitting were calculated for k = 1.5−11.5 Å^{-1}.

Quantitative analysis of eq 3 requires knowing $\phi_{as}(k)$, $A_{as}(k)$, S, and λ for each absorber−scatterer pair. The fits presented in this work used phase and amplitude functions derived using both the single-scattering (version 3.25) and the multiple-scattering (version 5.05) versions of FEFF, a computer program that calculates these functions according to curved wave theory.[80,81] R and σ were varied in the nonlinear least-squares-fitting algorithm. N_s was varied in the sense that all reasonable values of coordination number were tried in fixed coordination number fits. The optimum values for ΔE_0 and S were determined to be 10 eV (i.e., E_0 = 6545 eV) and 0.9, respectively, based on fits to several crystallographically characterized high-valent Mn dimers.[82] These parameters are consistent with values obtained for many other transition metal complexes and were held constant in subsequent fits. The k^3 weighted EXAFS data were used for all analyses to account for the decrease in EXAFS amplitude at high k.

The mean-square deviation, F, was used to judge the quality of fit.

$$F = \left[\sum k^6(\chi_{obs} - \chi_{calc})^2/N\right]^{1/2} \tag{4}$$

where N is the number of points in the spectrum and the summation is over all points in the spectrum. To account for the limited number of degrees of freedom in the fits, F was scaled to give

$$F' = F^2/\nu \tag{5}$$

where ν is defined as $N_{pts} - \rho$.[79] N_{pts} is the number of degrees of freedom and can be calculated as $N_{pts} = 2\Delta k\Delta R/\pi$, where Δk is the range (in Å^{-1}) over which the data are being analyzed and ΔR is the region (in Å) of the Fourier transform where the signal is found. ρ is the number of variables in each fit. For the present data, with Δk = 10 Å^{-1} and ΔR = 2.3 Å, $N_{pts} \sim 15$. For each shell, R and σ were the only variable parameters.

XANES data were normalized as previously described.[32] These spectra were then fit with linear combinations of Mn(II), Mn(III), and Mn(IV) model compounds. These models contain Mn with predominantly oxygen and nitrogen coordination spheres, as sulfur is not believed to be a ligand to the Mn in the OEC. The Mn(II) content can be determined with an uncertainty of approximately 10% using this method because of the distinctive shape of the Mn(II) XANES spectrum.[35,83]

Results

EXAFS of the S_1 State. Although EXAFS results for the control S_1 sample have been reported elsewhere by us[32] and others,[33,34] we show them here both for comparison with the reduced samples and because the present data represent a significant improvement in signal to noise over previously published spectra. The use of curved wave theoretical parameters[80,81] has allowed our analysis to extend to lower k data than in previous work. The EXAFS data for a single S_1 data set and the corresponding fits are shown in Figure 1. An independent control S_1 sample was studied for each reductant, in order to ensure that all results were reproducible. Consequently, a large number of control S_1 data sets have been

(76) Zhang, K.; Rosenbaum, G.; Bunker, G. *Jpn. J. Appl. Phys.* **1993**, *32*, 147−149.
(77) Cramer, S. P.; Tench, O.; Yocum, M.; George, G. N. *Nucl. Instrum. Methods* **1988**, *17266*, 586.
(78) Jenkins, R.; Gould, R. W.; Gedcke, D. *Quantitative X-ray Spectrometry*; Marcel Dekker, Inc.: New York, 1981.
(79) Lytle, F. W.; Sayers, D. E.; Stern, E. A. *Phys. B* **1989**, *158*, 701−722.
(80) Rehr, J. J.; Albers, R. C. *Phys. Rev.* **1990**, *B41*, 8139.
(81) Rehr, J. J.; de Leon, J. M.; Zabinsky, S. I.; Albers, R. C. *J. Am. Chem. Soc.* **1991**, *113*, 5135−5140.
(82) Riggs-Gelasco, P.; Gelasco, A.; Kitajima, N.; Armstrong, W.; Pecoraro, V.; Penner-Hahn, J. Manuscript in preparation.
(83) Waldo, G. S. Ph.D. Thesis, University of Michigan, 1991.

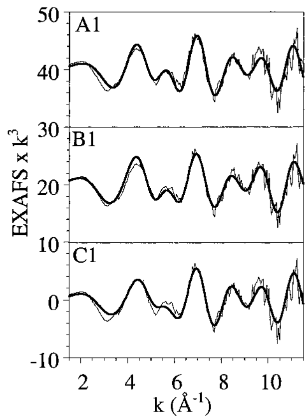

Figure 1. Unfiltered EXAFS data (thin lines) and associated fits (bold lines) of a single control S_1 data set. Fit A1 is the best fit using 3 shells of scatterers. Fit B1 shows the improvement obtained by using 2 shells of oxygen nearest neighbors along with the 2 shells of Mn. Fit C1 shows the improvement seen with the addition of Cl. All spectra are plotted on the same scale and are offset vertically for clarity. All fits were done over the k range 1.5−11.5 Å^{-1}. See Table 2 for best fit parameters.

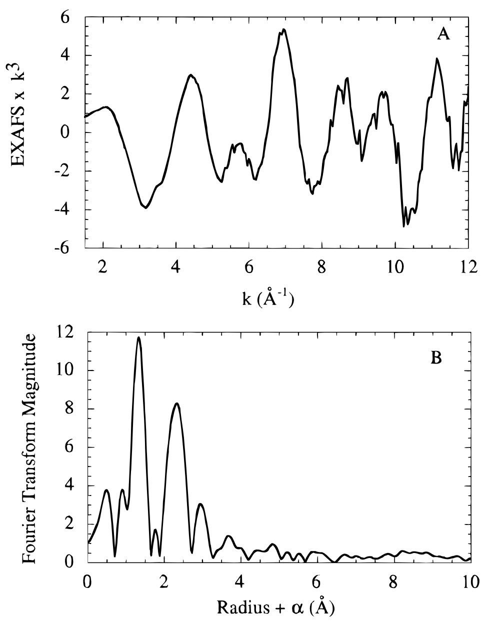

Figure 2. Average of the EXAFS for five independent control S_1 samples (part A) and resulting Fourier transform over the k range 1.5−12 Å^{-1} (part B).

collected. All of the S_1 data sets appear to be identical within the noise level of the data and an average of the five best data sets is shown in Figure 2A with the resulting Fourier transform in Figure 2B. For comparison, the Fourier transform of a single control data set is shown in the control experiment of Figure 3.

As previously noted, the principal peaks in the Fourier transform are at 1.4, 2.3, and 3.0 Å (note that these peaks correspond to interactions at ca. 1.8, 2.7, and 3.3 Å).[32−34,84] The small peak between the two principal features at 1.4 and 2.3 Å is most likely an artifact of the Fourier transformation, as its presence is dependent upon the method used for background removal. Peaks at lower R are low-frequency noise arising from incomplete background removal and can be altered by varying the method of background subtraction. None of the principal features at higher R depend on background removal. In an earlier report, we suggested that there might be an additional

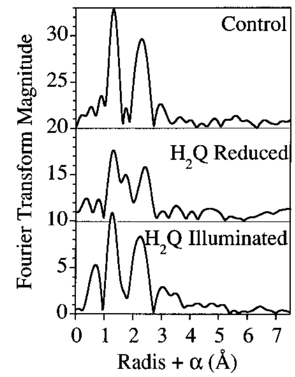

Figure 3. Fourier transforms of hydroquinone treated OEC. Top frame: Control S_1 state. Middle frame: Hydroquinone reduced sample. Bottom frame: Reduced sample after continuous illumination and a period of dark adaptation. Data range for FT is 1.5−11.5 Å^{-1}.

peak at about 4 Å.[32] By averaging five separate S_1 data sets, a poorly resolved peak can be seen at 3.8 Å (Figure 2). This peak appears to be present in all of the individual data sets, but it is only clearly above the noise level for 2 out of the 5 individual data sets.

The curve fitting results for six control S_1 samples are summarized in Table 1. Fits to both the unfiltered data and the data filtered over a wide R range ($R \approx 0.8-3.3$ Å) are included. The latter give nearly identical results, but have lower levels of high-frequency noise. As shown in Table 1, the reproducibility of the data is excellent when fit with three shells of scatterers. Although the accuracy of the distance determination is estimated to be ± 0.02 Å for the first and second shells and ± 0.05 Å for the third shell distances,[85] the precision of the experiment is much better. Despite the fact that samples were prepared over several years and studied using different facilities, the precision of the three-shell fits is approximately 0.005 Å for nearest neighbor and next-nearest neighbor distances.

It has been reported that the first shell of scatterers in the OEC can be resolved into short (1.81 Å) and long (1.95−2.16 Å) Mn−O (or N) distances.[30,34,86] In our initial report on the EXAFS of S_1, we found no evidence for this separation. With the availability of improved data and multiple data sets, we have re-examined this question. We find that while it is possible to fit the data with two different shells of oxygen nearest neighbors, the improvement in fit quality is extremely small (<20% in all cases). No improvement in fit quality (F') is obtained by including a shell of chlorine. Figure 1 illustrates this point graphically; it is clear that, except for $k < 3$ Å^{-1}, the three-shell fit reproduces all of the features of the data. The addition of the second oxygen shell gives a slight improvement for $k = 2.5-3.5$ Å^{-1} but makes the fit worse for $k = 3.5-4.5$ Å^{-1}.

For fits using a single Mn−O shell, the average Mn−O distance obtained for 6 different control data sets was 1.849 ± 0.003 Å with an apparent average coordination number of 2−3 O(N) per Mn. Table 2 lists the fit parameters for the fits to the single control data set shown in Figure 1. It is noteworthy that the refined Mn-O parameters show significantly increased variability in the fits using two Mn−O shells (Table 1). These are the only parameters that vary between the filtered and the unfiltered data. This behavior most likely results from the fact that the two different Mn−O shells are separated by less than the resolution of the data. Thus, small variations in the data

(84) DeRose, V. J.; Mukerji, I.; Latimer, M. J.; Yachandra, V. K.; Sauer, K.; Klein, M. P. *J. Am. Chem. Soc.* **1994**, *116*, 5239−5249.

(85) Teo, B. K. *EXAFS: Basic Principles and Data Analysis*; Springer-Verlag: New York, 1986; Vol. 9.

(86) McDermott, A. E.; Yachandra, V. K.; Guiles, R. D.; Cole, J. L.; Dexheimer, S. L.; Britt, R. D.; Sauer, K.; Klein, M. P. *Biochemistry* **1988**, *27*, 4021−4031.

Table 1. Average Fit Parameters to Six Control (S_1) Samples[a]

unfiltered data			filtered data				
shell[c]	R (Å) (dev)	σ^2 (dev)[d]	shell	R (Å) (dev)	σ^2 (dev)	F[b]	F'
3 O	1.849(3)	6.1(4)	2−4 O	1.848(6)	5.6(23)		
1−1.5 Mn	2.720(4)	1.2(8)	1.0−1.5 Mn	2.720(4)	1.3(7)		
0.5−1 Mn	3.255(18)	5.5(24)	0.5−1.0 Mn	3.256(12)	8.1(22)	0.485	0.0223
2−3 O	1.818(14)	1.9(16)	2−3 O	1.822(10)	2.4(13)		
1−2 O	1.977(28)	4.2(19)	1−2 O	1.987(22)	4.2(17)		
1−1.5 Mn	2.725(6)	1.6(14)	1−1.25 Mn	2.725(4)	1.6(9)		
0.5−1 Mn	3.266(30)	7.1(25)	0.5−1 Mn	3.261(19)	8.6(16)	0.395	0.0182
2−4 O	1.847(8)	5.3(27)	2−3 O	1.849(4)	5.1(16)		
0.5−1 Cl	2.550(22)	2.2(13)	0.5 Cl	2.540(18)	2.0(16)		
1.25−1.75 Mn	2.706(3)	3.8(16)	1−1.75 Mn	2.707(4)	2.9(18)		
0.5 Mn	3.263(28)	4.2(11)	0.5−1.0 Mn	3.256(25)	8.8(15)	0.457	0.0244

[a] Distances and σ^2 values are average values obtained for the best fits to six independent control data sets. Coordination numbers are listed as the range of values obtained in the best fits in the six data sets. The uncertainty (standard deviation) in the last digit for R and σ is given in parentheses. This represents the reproducibility between data sets and not the estimated accuracy (see text). [b] F and F' values are for fits to filtered data of the average of 6 data sets. The k range was 1.5−11.5 Å^{-1} and the filter range was 0.7−3.3 Å. [c] Coordination numbers were varied in the sense that all reasonable values were tried by incrementing through a range of fixed values. Oxygen values were stepped from 1, 2, ..., 6 with all permutations for the two shell oxygen fits. The Mn coordination number at 2.7 Å was fixed at 0.75, 1.0, 1.25, 1.5, or 1.75. The Mn coordination number at 3.3 Å was fixed at 0.25, 0.5, 0.75, or 1.0. Cl coordination numbers were fixed either at 0.5 or 1.0. [d] σ^2 is in units of Å^2 × 10^3.

Table 2. Fits to a Single Control (S_1) Data Set

unfiltered fits				filtered fits (1-3.3 Å)			
shell	R (Å)	σ^2 [a]	fit[b]	shell	R (Å)	σ^2	fit
3 O	1.84	5.9	A1	3 O	1.85	6.2	A2
1.5 Mn	2.72	2.3		1.5 Mn	2.72	2.5	$F' = 0.070$
0.5 Mn	3.26	3.5	$F = 1.139$	0.5 Mn	3.26	3.9	$F = 0.774$
2 O	1.81	0.2	B1	3 O	1.82	3.5	B2
2 O	1.96	3.0		2 O	2.00	5.3	
1 Mn	2.73	0.2		1 Mn	2.73	0.5	$F' = 0.068$
1 Mn	3.25	9.1	$F = 0.978$	1 Mn	3.25	9.4	$F = 0.668$
2 O	1.85	5.9	C1	3 O	1.85	6.1	C2
0.5 Cl	2.53	0.6		0.5 Cl	2.53	0.1	
1 Mn	2.71	1.1		1.25 Mn	2.71	2.8	$F' = 0.076$
0.5 Mn	3.23	5.5	$F = 1.091$	0.5 Mn	3.25	6.1	$F = 0.706$

[a] σ^2 is in units of Å^2 × 10^3. [b] Fits A1, B1, and C1 are shown in Figure 1 for comparison with the unfiltered data.

can lead to large changes in the apparent Mn−O distance. This supports our suggestion that there is only one *resolvable* shell of Mn−O/N scatterers.

The second shell of data can be fit with 1−1.5 Mn···Mn interactions at 2.720 ± 0.004 Å. Inclusion of a second scatterer (either C, Mn, or Cl) at 2.5−3 Å does not improve the fit significantly in either the filtered or unfiltered data. With several control data sets to compare, we have noticed that the coordination number of the 2.7 Å peak is dependent on the k range used for data analysis. Inclusion of data from 1.5−3.0 Å^{-1} changes the best coordination number from CN values of 1.2−2.0 to lower CN values of 1.0−1.5.

The third-shell fits are more problematic since there are more potential scatterers at longer distances and since multiple scattering may become important at longer distances. Using single scattering theoretical models, the third peak can be fit with either Ca or Mn. Calcium fits refined to distances 0.05 Å longer than the corresponding Mn fits due to the differences in the phase functions for these two elements. In other regards, the two metals are sufficiently similar that they cannot be distinguished by EXAFS curve fitting. Based on metal substitution studies, we believe this peak is best described by Mn···Mn EXAFS.[87] The apparent Mn···Mn distances for the different data sets range from 3.24 to 3.29 Å.

(87) Riggs-Gelasco, P.; Mei, R.; Ghanotakis, D.; Yocum, C. F.; Penner-Hahn, J. E. *J. Am. Chem. Soc.* **1996**, *118*, 2400−2410.

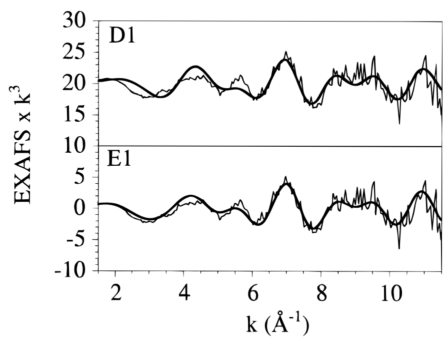

Figure 4. Unfiltered EXAFS data (thin lines) and associated fits (bold lines) of the hydroquinone reduced state (in the dark). Fit E1 (see Table 3) was obtained using 3 shells of scatterers over the k range 1.5−11.5 Å^{-1}. Fit D1 shows a 2-shell fit involving only Mn and a single shell of oxygen scatterers. Fit D1 is offset for clarity. See Table 3 for best fit parameters.

Hydroquinone Reduced Samples. We noted previously that incubation with hydroquinone causes a dramatic edge shift to lower energy.[35] As expected, the H_2Q treated sample also displays pronounced changes in the EXAFS data.[88] The unfiltered EXAFS data and corresponding fits are shown in Figure 4, the resulting Fourier transform is shown in Figure 2B, and fit parameters are summarized in Table 3. The most noticeable changes are the decreased amplitude in the first Fourier transform peak and the increased amplitude in the peak at 1.8 Å. The 2.7 Å Mn···Mn shell is roughly one-half of its original amplitude, and the 3.3 Å feature is no longer discernible above the noise level. These observations are qualitatively consistent with the reduction of about one-half of the Mn to Mn(II), since Mn(II) is expected to have longer Mn−O bonds and is not expected to form oxo-bridged dimers with 2.7 Å Mn···Mn distances. In contrast with our results for the S_1 state, two shells of Mn−O scatterers are required to fit the data for the H_2Q-treated sample. The goodness of fit, F', decreases by more than a factor of 2 in all cases. Fit D1 shows a two-shell fit utilizing a single shell of oxygen and manganese; fit E1 in Figure 4 is to unfiltered data using two oxygen shells and the Mn shell. The short Mn−O distance is slightly longer than that seen in the control S_1 data. The long Mn−O distance is

(88) The edge shifts for the H_2Q and NH_2OH reduced samples and their corresponding illuminated samples are identical to the edge shifts reported in reference 35.

Table 3. Fits to Hydroquinone Treated Samples (Dark)[a]

single data set								av fit refinements for three H_2Q data sets (filtered)		
unfiltered fits				filtered fits (1−2.85 Å)						
shell	R (Å)	σ^2 [b]	fit[c]	shell	R (Å)	σ^2	fit	shell	R (Å) (dev)[d]	σ^2 (dev)
2 O	1.85	4.0	D1	2 O	1.85	3.7	$F' = 0.069$	2−3 O	1.848(4)	5.0(1.0)
1 Mn	2.74	3.5	$F = 1.19$	1 Mn	2.74	4.2	$F = 0.732$	0.75−1.0 Mn	2.734(14)	2.7(1.5)
3 O	1.87	7.4	E1	2 O	1.86	3.7		2−3 O	1.875(7)	9.9(2.3)
2 O	2.18	5.7		2 O	2.16	10.4	$F' = 0.032$	2−3 O	2.174(4)	5.0(2.3)
0.75 Mn	2.74	1.5	$F = 1.06$	1 Mn	2.74	4.4	$F = 0.428$	0.7−1.0 Mn	2.734(7)	2.5(0.4)

[a] Fits to corresponding control are summarized in Table 2. [b] σ^2 is in units of Å^2 × 10^3. [c] Fits D1 and E1 are shown in Figure 4 for comparison with the unfiltered data. [d] The uncertainty (standard deviation) in the last digit is given in parentheses. This represents the reproducibility between data sets and not the estimated accuracy (see text).

Table 4. Fits to Hydroquinone Treated Sample (Illuminated)[a]

unfiltered fits				filtered fits (1.0-3.8 Å)			
shell	R (Å)	σ^2 [b]	fit[c]	shell	R (Å)	σ^2	fit
4 O	1.86	11.6	F1	4 O	1.87	11.2	$F' = 0.069$
1.25 Mn	2.71	2.7		1.25 Mn	2.71	2.3	
0.5 Mn	3.32	6.7	$F = 1.37$	0.5 Mn	3.32	5.1	$F = 0.904$
2 O	1.78	2.7		2 O	1.79	1.0	$F' = 0.082$
3 O	1.95	3.6		3 O	1.95	3.2	
1 Mn	2.71	1.5		1.0 Mn	2.72	1.4	
1 Mn	3.29	11	$F = 1.33$	0.5 Mn	3.32	3.6	$F = 0.896$

[a] Fits to corresponding control are summarized in Table 2. [b] σ^2 is in units of Å^2 × 10^3. [c] Fit F1 is shown in Figure 5 for comparison with the unfiltered data.

typical of those found for Mn(II). As suggested by the Fourier transform, the apparent Mn···Mn coordination number decreases by roughly one-third to one-half on H_2Q treatment. In addition, the Mn···Mn distance increases by 0.02−0.03 Å following H_2Q treatment.

One H_2Q data set was collected for a sample that was quenched by addition of ferricyanide prior to centrifugation and freezing; two data sets were also collected for samples which were quenched by centrifugation and freezing. The latter have a slightly lower edge energy (data not shown), suggesting that for these samples, the reduction reaction continued throughout the sample preparation. However, the shift in edge energy is small and there are only minor changes in the curve-fitting results as illustrated by the small standard deviations in Table 3. The most significant change in the curve fitting is that the apparent Mn···Mn coordination numbers of centrifugation-quenched samples decrease in amplitude by 50% relative to the control, while they decrease by only one-third for samples quenched by $K_3Fe(CN)_6$ and centrifugation.

We have shown previously by XANES and EPR that the changes observed with H_2Q treatment can be completely reversed on illumination and that H_2Q-treated samples have only minor loss of activity.[35,67] Consistent with this, the EXAFS changes are also reversed on illumination, as shown graphically in Figure 3C. The 2.1 Å Mn−O interactions disappear, the amplitude of the 2.7 Å Mn···Mn interaction doubles and shifts to slightly lower R, and the 3.3 Å Mn···Mn interaction reappears. The fits for this sample are summarized in Table 4, and the best fit is shown in Figure 5. The data for the illuminated sample are noisier than the data for the control; this is most likely because the H_2Q-treated sample was diluted for the illumination.[89] Despite the increased noise, the changes resulting from reduction are clearly reversed after illumination. The data once again can be fit with either one or two shells of nearest neighbors with approximately equivalent fit indices (F').

(89) All samples were centrifuged for the same period of time (6 min) and thus the pellets for the diluted samples had a lower final Mn concentration.

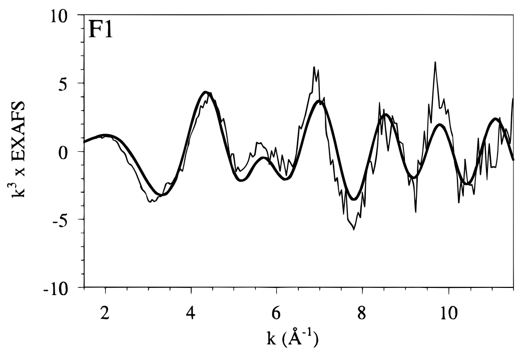

Figure 5. Unfiltered EXAFS data (thin line) and associated 3-shell fit of the illuminated, hydroquinone-treated sample (after dark adaptation). See Table 4 for fit details.

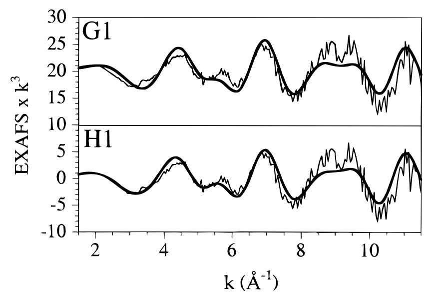

Figure 6. Unfiltered EXAFS data (thin line) and corresponding fits (bold lines) for the NH_2OH-treated sample. Fit G1 (offset vertically for clarity) is the 3-shell fit; fit H1 shows the improvement with 4 shells of scatterers. See Table 5 for fit details.

Also, the second shell fits refine to the shorter (2.71 Å) distance and both Mn···Mn shells return to their pre-reduction coordination numbers.

Hydroxylamine-Reduced Samples. We showed previously that non-inhibitory concentrations of NH_2OH give less dramatic edge shifts than does H_2Q.[35] Consistent with this, NH_2OH treatment gives only minor changes in the EXAFS spectrum.[88] The EXAFS spectrum of a NH_2OH-treated sample is shown in Figure 6 along with the best 3-shell and 4 shell fits. The corresponding Fourier transform is shown in Figure 7 in comparison to a control and a NH_2OH-treated and illuminated sample. Fitting results are summarized in Table 5. The principal change following NH_2OH reduction is a slight decrease in amplitude of the 2.7 Å Mn···Mn feature and a slight lengthening of the 3.3-Å interaction. Despite the appearance of change in the first peak in the FT, fitting results indicate that the first shell is very similar to that of the control. Inclusion of the second Mn−O shell gives only a modest (ca. 10%) decrease in F'. The longer Mn−O distance in the NH_2OH-treated samples (2.1 Å) is ~0.1 Å longer than the long Mn−O distances found in fits to the control. After illumination, the EXAFS of the control and of the NH_2OH-illuminated sample

Table 5. Fits to NH_2OH Reduced Samples[a]

single data set								av fit refinements for two NH_2OH data sets (filtered)		
unfiltered fits				filtered fits (1−3.3 Å)						
shell	R (Å)	σ^2 [b]	fit[c]	shell	R (Å)	σ^2	fit	shell	R (Å) (dev)[d]	σ^2 (dev)
3 O	1.84	2.7	G1	3 O	1.85	2.5	G2	3 O	1.859(20)	5(3)
1.0 Mn	2.73	2.2		1.0 Mn	2.73	1.9	$F' = 0.149$	1 Mn	2.731(7)	3(1)
0.5 Mn	3.28	4.6	$F = 1.72$	1.0 Mn	3.27	8.8	$F = 1.13$	0.5-1 Mn	3.26(1)	14(6)
3 O	1.84	2.0	H1	3 O	1.7		H2	3 O	1.864(18)	4(4)
2 O	2.08	11.8		1 O	2.08	0.7		1−2 O	2.16(11)	8(1)
1 Mn	2.73	2.5		1 Mn	2.73	2.7	$F' = 0.137$	1 Mn	2.731(7)	3(1)
0.5 Mn	3.28	4.8	$F = 1.61$	1 Mn	3.27	9.8	$F = 0.95$	0.5−1 Mn	3.26(1)	14(6)

[a] Fits to corresponding control are summarized in Table 2. [b] σ^2 is in units of $Å^2 \times 10^3$. [c] Fits G1 and H1 are shown in Figure 6 for comparison with the unfiltered data. [d] The uncertainty (standard deviation) in the last digit is given in parentheses. This represents the reproducibility between data sets and not the estimated accuracy (see text).

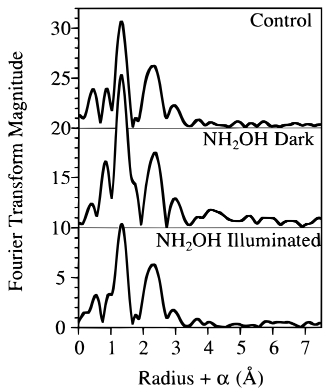

Figure 7. Fourier transform of EXAFS data for a control S_1 sample (top frame), a NH_2OH-treated sample (middle frame), and for a sample treated with NH_2OH and then illuminated (bottom frame). Data sets transformed using a k range of 1.5−11.5 $Å^{-1}$.

Table 6. Comparison of Fits for a NH_2OH Illuminated Sample vs the Corresponding Control S_1

unfiltered fits				filtered fits[b]			
shell	R (Å)	σ^2 [a]	fit	shell	R (Å)	σ^2	fit
Control S_1							
3 O	1.86	7.6	$F = 0.843$	3 O	1.86	7.7	$F = 0.552$
1.0 Mn	2.73	2.6		1 Mn	2.73	2.5	
0.5 Mn	3.25	3.1		0.5 Mn	3.25	2.8	$F' = 0.035$
1 O	1.81	0.9	$F = 0.793$	3 O	1.85	5.5	$F = 0.550$
3 O	1.91	12.1		1 O	2.04	4.4	
1 Mn	2.73	2.9		1.25 Mn	2.73	4.5	
0.5 Mn	3.25	4.4		0.5 Mn	3.26	3.7	$F' = 0.046$
NH_2OH illuminated							
3 O	1.86	7.2	$F = 0.687$	3 O	1.86	7.4	$F = 0.375$
1 Mn	2.27	2.5		1 Mn	2.73	2.6	
0.5 Mn	3.24	3.8		1 Mn	3.25	4.5	$F' = 0.014$
3 O	1.85	5.3	$F = 0.635$	3 O	1.85	6.4	$F = 0.324$
1 O	2.04	5.5		1 O	2.04	11	
1 Mn	2.73	3.0		1 Mn	2.73	2.8	
0.5 Mn	3.24	5.0		1 Mn	3.25	10	$F' = 0.013$

[a] σ^2 is in units of $Å^2 \times 10^3$. [b] Filter range for control = 1−3.3 Å; filter range for NH_2OH reduced and illuminated sample = 0.8−3.3 Å.

are indistinguishable. Fits to the NH_2OH-illuminated sample and the corresponding control are compared in Table 6.

Hydroxylamine Titrations. Treatment with 100 μM NH_2OH for 3 min results in reduction based on a small edge shift but does not result in Mn loss or activity loss.[35] These were the conditions employed for the EXAFS studies above, since under these conditions, reduction is maximized without Mn loss. In order to understand further the reduction reactions and the differences between H_2Q and NH_2OH reductions, we measured the XANES spectra for samples treated with increasing concentrations of NH_2OH (50, 100, 150, 200, and 400 μM) for 3 min and for samples treated with 100 μM NH_2OH for varying incubation times (1,3,5,7,9, or 12 min). These normalized edges are presented in Figures 8 and 9. As expected, the edges shift to lower energies as the NH_2OH treatments become more drastic, indicating production of Mn(II). The data in Figures 8 and 9 are normalized to reflect the absorbance per Mn atom. This normalization permits direct comparison of the average Mn environment, but masks the fact that the intensity of the Mn fluorescence decreases with increasing NH_2OH concentration or incubation time. The *unnormalized* step height (i.e., the number of Mn Kα fluorescent photons detected above the Mn edge) decreases monotonically as the NH_2OH treatment becomes harsher. Since edge height is proportional to the

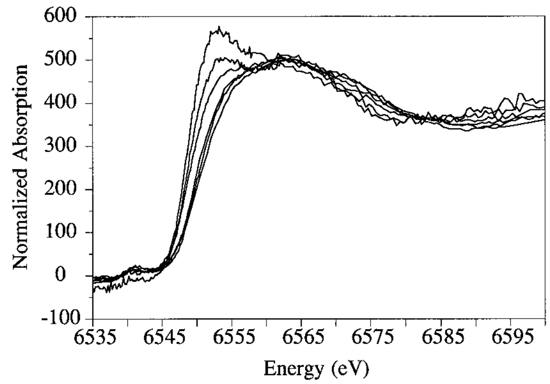

Figure 8. XANES spectra for samples treated at various NH_2OH concentrations. After 3 min, samples were quenched by 40-fold dilution into a $CaCl_2$/MES buffer. From left to right, NH_2OH concentrations are 400, 250, 150, 100, 50, and 0 μM. Spectra have been normalized to a constant edge jump per Mn.

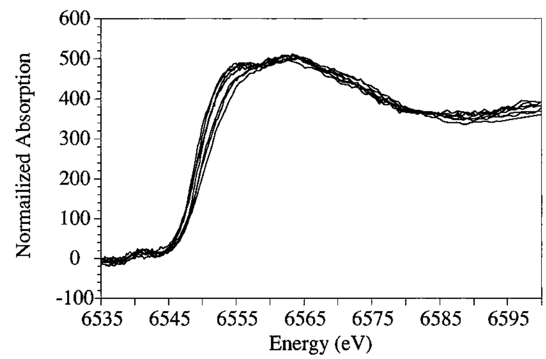

Figure 9. XANES spectra for samples treated for various times with 100 μM NH_2OH. After the appropriate incubation period, samples were quenched with a 40-fold dilution into a $CaCl_2$/MES buffer. From left to right, incubation times were 12, 9, 7, 5, 3, 1, and 0 min. Spectra have been normalized to a constant edge jump per Mn.

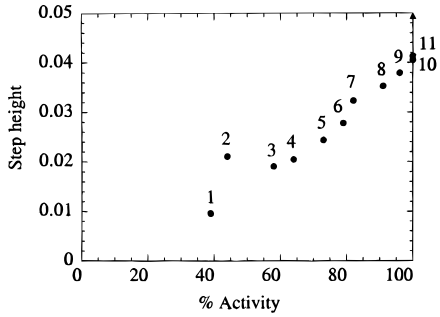

Figure 10. Relationship between step height and activity for NH_2-OH-treated samples for spectra shown in Figures 8 and 9. Circles: NH_2-OH-treated samples that were diluted prior to pelleting. Point 1 is 400 μM NH_2OH for 3 min; point 2 is 100 μM NH_2OH for 12 min; point 3 is 250 μM NH_2OH for 3 min; point 4 is 100 μM NH_2OH for 9 min; point 5 is 100 μM NH_2OH for 7 min; point 6 is 150 μM NH_2OH for 3 min; point 7 is 100 μM NH_2OH for 5 min; point 8 is 100 μM NH_2-OH for 3 min; point 9 is 50 μM NH_2OH for 3 min; point 10 is 100 μM NH_2OH for 1 min; point 11 is for 100 μM NH_2OH for 0.5 min. Triangle: Control sample that was not diluted prior to pelleting. Step heights were calculated by extrapolating a line from the EXAFS region through the absorption edge. Activities are upper limits of activity based on assays performed immediately after quenching the reaction. Percent activity is defined relative to the control S_1 state (1370 μmol of O_2/mg of chl/h).

amount of Mn that is retained in the pellet, this means that Mn is released from the samples that are treated under harsher conditions. The unnormalized step heights are compared to activity in Figure 10. The observed activity depends linearly on Mn concentration and extrapolates to approximately zero activity when all Mn is lost.

Discussion

First Shell of Control. The acquisition of lower noise EXAFS data for the S_1 state has permitted a reexamination of fits for this state. The apparent Mn−O distances are somewhat shorter than those that we reported previously.[32] This is most likely due to the fact that our present fits utilize *ab initio* parameters while our earlier work utilized empirical Mn−O parameters derived from a distorted Mn(III) complex.[32] We had suggested previously that there were not two resolvable shells of nearest neighbors around the Mn. However, there have been recent reports indicating that the first shell requires both short, 1.8 Å, Mn−O distances and longer, 2.0 Å, Mn−O/N distances, although there is considerable variation in the apparent long Mn−O distance (1.90−2.25 Å).[29,34,63,84,90]

The fit index F does not penalize for the use of additional shells of scatterers. The International Commission on Standards and Criteria in X-ray absorption spectroscopy[79] has suggested using a statistic analogous to a reduced χ^2 to quantitate errors associated with models using ρ variable parameters (eq 6).

$$\epsilon^2 = \frac{(N_{idp}/\nu)\sum_{i=1}^{N}(\chi_{obs}(k_i) - \chi_{calc}(k_i))^2/\sigma_i^2}{N} \qquad (6)$$

The sum is calculated over all of the measured data points, N, and the error at each point is weighted by $1/\sigma_i^2$, where σ_i is the rms uncertainty in χ_{obs}. The $1/\nu$ weighting introduces a penalty for adding additional, unjustified, shells of scatterers. This statistic has proven difficult to calculate for EXAFS because σ_i^2 includes contributions from both statistical and nonstatistical errors.[79] As an approximation to ϵ^2, we have calculated F' (eq 5). F' provides an improved estimate of the significance of a fit, but because it omits the $1/\sigma_i^2$ weighting, F' is not an ideal measure of the error. In particular, omitting the $1/\sigma_i^2$ term makes F′ more sensitive to noise than ϵ^2. For unfiltered fits, the high-frequency noise dominates F', making changes due to the quality of the model negligible. For this reason, we have only used F' with filtered data.

For most of the control and NH_2OH data sets, there is a small decrease in F' on including a second Mn−O/N shell. For the six control data sets, the average decrease in F' is 12% . Is 12% a *significant* improvement? If F' were a true χ^2 statistic, a significant improvement at the 95% confidence level would require >40% decrease in F'.[91] Based on this, a 12% improvement is not significant. However, given the known limitations of F', we have preferred to rely on crystallographically characterized di-μ-oxo bridged models to determine the expected improvement in F'.[82] To address this question, we have analyzed the EXAFS of several crystallographically characterized models.[82] For models that are known to have two distinct shells of nearest neighbors, $[Mn^{III}/Mn^{IV}(O)_2(2,2'\ bipyridine)_2]$,[92] $[Mn^{III}(HB(3,5\text{-}iPr_2pz)_3)]_2(O)_2$,[93] and $[Mn(HB(3,5\text{-}iPr_2pz)_3)]_2(O)_2$-(OAc),[39] the ratios of F'(one shell of nearest neighbors) to F'-(two shells of nearest neighbors) are 2.5, 6.8, and 3.5 respectively. For superoxidized Mn catalase, the ratio is 2.4.[94,95] In contrast, models that lack well-defined shells, $[Mn_4O_2(tphpn)_2$-$(H_2O)_2(ClO_4)_2](ClO_4)_3$[96] and $[Mn^{IV}(\mu\text{-}O)(salpn)_2]_2$,[97] have F' ratios of 0.9 and 0.7, respectively for inclusion of additional shells. Although these models have both short Mn−O distances (∼1.8 Å) and long Mn−(O/N) distances (∼2.1 Å), they also contain intermediate-range Mn−O interactions at 1.9 Å. The F' ratio for this second class of models is comparable to that observed for control OEC samples (average 1.1; maximum 1.2) and the NH_2OH-treated OEC samples (1.1).

A second line of evidence suggesting that two shells of nearest neighbors do not provide a good description of the OEC is the observation that the excellent precision seen in Table 1 for 3-shell fits is lost when an additional shell of oxygens is added. This suggests that a single minimum is not present on the four-shell error surface. This may account in part for the wide range of terminal ligand distances (1.90−2.25 Å) that have been reported in other studies.[29,34,63,84,90]

Although a single Mn−O shell provides a minimal model for the EXAFS oscillations, the single Mn−O fit is not chemically satisfactory. The apparent Mn−O distance (1.85 Å) is too long for the expected $Mn-O_{oxo}$ distance (≈1.8 Å) and far too short for the expected *average* Mn−nearest neighbor distance. In addition, the apparent Mn−O coordination numbers (ca. 3 oxygens at 1.85 Å) are far too low. In this context, it is important to remember that the lack of significant improvement

(90) MacLachlan, D. J.; Hallahan, B. J.; Ruffle, S. V.; Nugent, J. H. A.; Evans, M. C. W.; Strange, R. W.; Hasnain, S. S. *Biochem. J.* **1992**, *285*, 569−576.

(91) Bevington, P. R. *Data Reduction and Error Analysis for the Physical Sciences*; McGraw-Hill: New York, 1969; pp 187−203. Using the F test for $P(F, \nu_1, \nu_2) = 0.05$ with $\nu_1 = 2$ and $\nu_2 = N_{pts} - 8 \approx 8$, where $F = \{[\chi^2(3\text{ shell}) - \chi^2(4\text{ shell})]/\nu_1\}/\{\chi^2(4\text{ shell})/\nu_2\}$.

(92) Plaksin, P. M.; Stoufer, R. C.; Mathew, M.; Palemik, G. J. *J. Am. Chem. Soc.* **1972**, *94*, 2121.

(93) Kitajima, N.; Osawa, M.; Imai, S.; Moro-oka, Y. Submitted for publication.

(94) Waldo, G. S.; Yu, S.; Penner, H. J. E. *J. Am. Chem. Soc.* **1992**, *114*, 5869−70.

(95) Stemmler, T.; Sturgeon, B. E.; Randall, D. W.; Britt, R. D.; Penner-Hahn, J. E. Manuscript in preparation.

(96) Chan, M. K.; Armstrong, W. H. *J. Am. Chem. Soc.* **1990**, *112*, 4985−4986.

(97) Larson, E. J.; Pecoraro, V. L. *J. Am. Chem. Soc.* **1991**, *113*, 7809−7810.

on adding a second shell of oxygens does not mean that no oxygens are present at ~2 Å. It means only that the model using two shells of nearest neighbors does not provide a significantly improved description of the EXAFS.

This result is characteristic of disordered Mn complexes. Thus, for example, the EXAFS data for $[Mn^{IV}(salpn)(\mu\text{-}O)]_2$ dimer[98] are best fit by a *single* shell of 3−4 Mn−O scatterers at ~1.90 Å, despite the presence of both short $Mn-O_{oxo}$ distances and longer Mn−O/N distances.[99] Likewise, $[Mn_4O_2(tphpn)_2(H_2O)_2(ClO_4)_2](ClO_4)_3$ is best fit with two shells of Mn−O/N at 1.88 and 2.20 Å; fits utilizing three shells of nearest neighbors (1.79, 1.95, and 2.20 Å) do not decrease F', despite the fact that they are a better description of the distribution. This stands in contrast to the results for other Mn dimers and for oxo-bridged dinuclear Fe proteins where Fe−O and Fe−N distances are readily resolvable.[100] The difference lies in the distribution of distances. As noted above, models such as $[Mn^{IV}(salpn)(\mu\text{-}O)]_2$ and $[Mn_4O_2(tphpn)_2(H_2O)_2(ClO_4)_2](ClO_4)_3$ have Mn−O distances of ~1.9 Å in addition to shorter $Mn-O_{oxo}$ and longer Mn−O/N distances.

Unfortunately, the resolution of the present OEC data (ΔR ~ 0.16 Å) is not sufficient to justify the use of three shells of nearest neighbors. For $[Mn^{IV}(salpn)(\mu\text{-}O)]_2$, the true Mn−ligand distribution is not well described by a simple two-shell distribution and thus it is not surprising that the two-shell distribution fails to give a significant improvement in F'. A similar situation may exist for the OEC, where Mn−O distances of ~1.9 Å could come from hydroxo, alkoxo, or phenoxo ligation. However, in the absence of either additional information about the Mn−ligand distribution or improved resolution in the EXAFS, it will be difficult to provide a unique description of the Mn−ligand distances. For the present, we present a minimal description of the EXAFS (~3 Mn−O at 1.85 Å) together with a recognition that the existence of the chemically unreasonable result must reflect disorder in the Mn site.

Outer Shells of the Control. Accurate characterization of the Mn···Mn interactions at ca. 2.7 Å is critical for constructing a structural model of the OEC. This distance is characteristic of di-μ-oxo bridged dimers. The apparent Mn···Mn coordination numbers range from 1.0 to 1.5 with an average of 1.25. This would appear to reflect the presence of two or three Mn···Mn interactions at ca. 2.7 Å. If this shell is disordered, a true Mn···Mn coordination number of 1.5 (i.e., three Mn···Mn interactions) could give rise to an apparent Mn···Mn coordination number of 1.25. However, two additional complications are possible for the 2.7-Å peak that were not possible for the first shell. At this distance, multiple scattering could affect the observed EXAFS. It is also possible that Mn···C EXAFS (e.g. from a bidentate carboxylate) could contribute to the observed 2.7-Å peak. Simulations using FEFF 5.0 and reasonable $Mn_2(\mu\text{-}O)_2$ geometries suggest that multiple-scattering pathways are not important for the 2.7-Å peak. We are not able to resolve a separate Mn···C shell; however, this does not prove that there is no Mn···C component at 2.7 Å. If present, Mn···C scattering could lead to a slight overestimate of the Mn···Mn coordination number, thus allowing two Mn···Mn interactions to give an apparent coordination number of 1.25. Given these complications, it is not possible with the present data to determine whether there are two or three Mn···Mn interactions.

The observed Mn···Mn distance is typical of unsupported di-μ-oxo bridged dimers, and is somewhat longer than those seen in triply-bridged species (e.g. $Mn_2(\mu\text{-}O)_2(\mu\text{-carboxylato})$).[101] The Mn···Mn distance in the OEC is 0.1 Å shorter than that in (μ-oxo)(μ-hydroxo) bridged dimers[102] and 0.4 Å longer than that in $(\mu\text{-}O)_3$ bridged dimers.[103] Consequently, it appears most likely that the OEC contains two or three $Mn_2(\mu\text{-oxo})_2(\mu\text{-carboxylato})_n$ (n = 0, 1) structures. We presently favor a model with two such dimers because in order to have three Mn···Mn interactions with only four Mn, one of the Mn would have to participate in two $Mn_2(\mu\text{-oxo})_2$ dimers. Several inorganic analogues having such a structure have been synthesized.[104−106] In the models prepared to date, the average Mn···Mn distance is ≥2.75 Å and, thus, somewhat longer than that seen in the OEC.

The third shell of the control is best fit with either Mn···Mn or Mn···Ca interactions. Addition of a shell of C at ≈3 Å gives an improvement in the fit as judged by F without changing the apparent Mn···(Mn/Ca) distance or coordination number. However, F' calculations indicate that the putative Mn···C shell at ≈3 Å makes too small of a contribution to the overall EXAFS to be reliably refined (ratio of F'(3 shell fit) to F'(3 shell fit + C) ~ 0.9). Given the disordered nature of the likely ligand environments, this is not surprising.

EXAFS of Reduced Derivatives. The reversibility of both the EXAFS structural changes and the XANES edge shifts in reduced PSII complexes points to the existence of stable, reduced states of the OEC. A potential difficulty in studying reduced samples is that any inactive centers that are formed could contribute a spurious signal from adventitiously bound Mn. In our samples, the presence of 10 mM Ca(II) should displace any adventitiously bound Mn.[4] This is confirmed by the correlation of activity with Mn concentration (Figure 10). The amount of Mn remaining in PSII pellets decreases linearly with decreasing activity, thus demonstrating that under our conditions, essentially all of the Mn that is present in the XAS samples is present in active OEC centers. This is consistent with the complete photoreversibility of the observed changes.

The H_2Q-reduced samples show dramatic structural changes. The decrease in the apparent coordination number for the 1.85 Å Mn−O shell and the presence of a new Mn−O shell at ca. 2.16 Å are both consistent with the reduction of Mn(III) or Mn(IV) to Mn(II), since Mn(II) complexes have significantly longer average bond lengths than do Mn(III) or Mn(IV) complexes. The EXAFS results thus support earlier EPR[67] and XANES [35] evidence for the formation of Mn(II) following H_2Q reduction. The fits to the hydroquinone reduced sample indicate that the apparent number of Mn···Mn interactions at 2.7 Å is decreased to half that of the control. The simplest explanation for this is that one of the $Mn_2(\mu\text{-}O)_2$ units has been disrupted by the formation of Mn(II). This is consistent with the expectation that oxo bridged Mn(II) dimers would not be stable.

(98) Larson, E.; Lah, M. S.; Li, X.; Bonadies, J. A.; Pecoraro, V. L. *Inorg. Chem* **1992**, *31*, 373−378.

(99) Baldwin, M. J.; Stemmler, T. L.; Riggs-Gelasco, P. J.; Kirk, M. L.; Penner-Hahn, J. E.; Pecoraro, V. L. *J. Am. Chem. Soc.* **1994**, *116*, 11349−11356.

(100) Sanders-Loehr, J. In *Iron Carriers and Iron Proteins*; Loehr, T. M., Ed.; VCH Publishers, Inc.: New York, 1989; pp 373−466.

(101) Larson, E. J.; Pecoraro, V. L. In *Manganese Redox Enzymes*; Pecoraro, V. L., Ed.; VCH Publishers: New York, 1992; pp 1−28.

(102) Larson, E. J.; Riggs, P. J.; Penner-Hahn, J. E.; Pecoraro, V. L. *J. Chem. Soc., Chem. Commun.* **1992**, 102−103.

(103) Wieghardt, K.; Bossek, U.; Nuber, B.; Weiss, J.; Bonvoisin, J.; Corbella, M.; Vitols, S. E.; Girerd, J. J. *J. Am. Chem. Soc.* **1988**, *110*, 7398−7411.

(104) Sessoli, R.; Tsai, H.-L.; Schake, A. R.; Wang, S.; Vincent, J. B.; Folting, K.; Gatteschi, D.; Christou, G.; Hendrickson, D. N. *J. Am. Chem. Soc.* **1993**, *115*, 1804−1816 and references therein.

(105) Philouze, C.; Blondin, G.; Girerd, J.-J.; Guilhem, J.; Pascard, C.; Lexa, D. *J. Am. Chem. Soc.* **1994**, *116*, 8557−8565.

(106) Dave, B. C.; Czernuszewicz, R. S. *New J. Chem.* **1994**, *18*, 149−155.

(107) Mukerji, I.; Andrews, J. C.; DeRose, V. J.; Latimer, M. J.; Yachandra, V. K.; Sauer, K.; Klein, M. P. *Biochemistry* **1994**, *33*, 9712−9721.

If the samples giving rise to the H_2Q EXAFS were a mixture of free Mn(II) and fully oxidized OEC in an approximate 1:1 ratio, the edge shift to lower energy, the Mn(II) quantitation, the new Mn−O distance at 2.2 Å, and the decrease in coordination number at 2.7 Å could all be rationalized. However, this scenario is inconsistent with the retention of activity and the photoreversibility of these samples. If half of the Mn were present as free Mn(II), there should be a 50% loss of activity in contrast to the observed retention of activity. Moreover, as noted above, free Mn(II) should remain in the supernatant, not in the pellet. We therefore conclude that the Mn(II) observed in this reduced sample is an integral part of the active complex, possibly trapped near its binding site. The fact that this Mn(II) is not displaced by Ca(II) suggests that it is sequestered within the protein matrix. This is consistent with the lack of proton relaxation enhancement for the hydroquinone treated sample and the fact that the reduced Mn is not EDTA extractable.[67]

The 3.3-Å feature is reversibly disrupted by H_2Q reduction. This is consistent with reduction of one or more of the Mn that are involved in this interaction. A simple model that can account for the observed changes in coordination number is the "dimer-of-dimers" model where two $Mn_2(\mu\text{-}O)_2$ units are linked by a single 3.3-Å Mn···Mn interaction.[34] Hydroquinone attack on one of the dimers would leave one intact dimer and two Mn(II). This model predicts apparent coordination numbers at 2.7 and 3.3 Å of 1.0 and 0.5 for S_1 and 0.5 and 0.0 for the H_2Q-reduced species. These correlate well with the observed coordination numbers. However, a redistribution of carbon density near 3.3 Å following H_2Q reduction could, in principle, cause the Mn···Mn component at 3.3 Å to be dampened, as a result of destructive interference between Mn···Mn and Mn···C scatterers. Consequently, we cannot rule out a reduction mechanism in which the 3.3-Å interaction is preserved following H_2Q treatment.

The 2.7-Å Mn···Mn distance shows a small but significant increase following H_2Q reduction. Although the accuracy of EXAFS bond lengths is ca. 0.02 Å, the precision (see Tables 1 and 2) is significantly better for the present samples. In model complexes, the Mn···Mn distance increases to ca. 2.8 Å when one μ-oxo bridge is protonated.[99] The observed Mn···Mn distance for the H_2Q-treated sample is thus probably too short to be due to a $Mn_2(\mu\text{-}O)(\mu\text{-}OH)$ core. If one of two Mn dimers is reduced by H_2Q, the change in bond length could reflect heterogeneity in the Mn···Mn distances for the S_1 state. That is, selective reduction of the dimer having the shorter Mn···Mn distance would lead to an increase in the apparent Mn···Mn distances. In a recent study of oriented PSII membranes, the 2.7-Å feature was found to be anisotropic, giving a distance of 2.71 Å at a 15° orientation and 2.74 Å at the 75° orientation.[107] Reduction of the former could give rise to our observed change in Mn···Mn distance. We cannot, of course, rule out the alternative that when H_2Q reduces one Mn dimer, it causes a structural perturbation in the other.

Hydroxylamine-Reduced Samples. The biggest changes in the Fourier transform for the NH_2OH-treated samples are a modest increase (20−40%) in the height of the nearest neighbor peak and a slight decrease (~15%) in the width of the 2.7-Å Mn···Mn peak. For multiple-shell compounds, the Fourier transform is a complex interference function that is difficult to interpret quantitatively.[79] Quantitative curve fitting (Table 5) demonstrates that the changes in the appearance of the Fourier transform are correlated with only small structural changes. The principal structural change that occurs following NH_2OH reduction is a decrease in the amplitude of the 2.7-Å Mn···Mn feature. This could be due to the loss of one out of three $Mn_2(\mu\text{-}O)_2$ dimers or to increased disorder in the Mn···Mn distances. As noted above, we favor a model having only two Mn···Mn distances at 2.7 Å. Within this model, reduction of Mn(IV) to Mn(III) by NH_2OH could increase the disorder in the Mn···Mn distances and thus account for the small decrease in the apparent amplitude of the 2.7-Å feature.

For fits using a single shell of Mn−O nearest neighbors, there are no significant differences in the nearest neighbor interactions between the control and the NH_2OH-treated samples. However, there *are* small changes in the fits using two Mn−O shells. In particular, the longer Mn−O distance increases by 0.1 Å. The improvement in F' on including this second shell is quite small, suggesting that, as with the control, this shell is not required by the data. Our interpretation of the NH_2OH nearest neighbor distributions follows that for the control. There must be several long (~1.9−2.2 Å) Mn−O/N distances which interfere destructively and which are not well modeled by a single "long" Mn−O shell. The long Mn−(O/N) distribution changes between the control and the NH_2OH-treated sample, as evidence by the change in the first Fourier transform peak and the change in apparent "long" Mn−O distances. It is not possible, with the present data, to provide a unique interpretation of these changes.

Reversible hydroxylamine reduction may or may not involve the formation of Mn(II). The XANES data can be fit either with Mn(III) alone or with a mixture of Mn(II) and Mn(IV).[35] However, the absence of significant structural changes following NH_2OH treatment suggests that Mn(II) is *not* formed since Mn(II) generally has very different structures from Mn(III) and Mn(IV). In particular, retention of the 2.7-Å peak appears to be most consistent with the $Mn(III)_4$ oxidation state assignment, since there are at present no known examples of 2.7-Å $Mn(\mu\text{-}O)_2Mn$ interactions involving Mn(II). The increase in the second Mn−O distance to ~2.1 Å for the NH_2OH-treated samples could be a consequence of the reduction of Mn(IV) to Mn(III), since tetragonally elongated Mn(III) would contribute longer Mn−O distances, thus shifting the outer Mn−O shell to longer distances.

In addition to the slightly reduced samples studied by EXAFS, a range of more reduced samples is accessible by hydroxylamine treatment. This is consistent with reports that S_{-2} and even S_{-3} states are formed by NH_2OH reduction.[57,58] As shown in Figure 10, production of these super-reduced states is accompanied by loss of Mn. That is, for states that are more reduced than S_{-1}, Mn loss begins to occur on a time scale comparable to reduction. In all likelihood, these super-reduced samples contain a mixture of S_{-1}, S_{-2}, S_{-3}, and inactive Mn-free reaction centers.

Reduction vs NH_2OH Binding in the Dark. In an earlier study, Guiles et al.[63] concluded that NH_2OH does not reduce the OEC in the dark but that reduction does occur after illumination. More recently, we have reported XANES evidence that NH_2OH does reduce the OEC in the dark.[35] The present data provide further support for the dark-reduction model. In particular, highly reduced samples can be produced by dark incubation with NH_2OH, in addition to the slightly reduced sample that we have characterized by EXAFS. The shifts in edge energy reported by Guiles et al. are comparable to those seen in Figures 8 and 9. By comparing Mn content with activity, we have shown that the Mn remaining in even the labile, highly reduced samples is associated with active centers and that inactive centers release Mn to the supernatant.

Guiles et al. observed a significant shift of the edge to lower energy when the NH_2OH-incubated samples were illuminated with a single flash. We observe a shift to higher energy (i.e.

photoreversibility) following continuous illumination. It may be that single flash illumination in the presence of NH_2OH (the conditions of Guiles et al.) leads to the production of NH_2OH radicals that are potent reductants. No NH_2OH was present during the photoreoxidation of our samples.

A Reduction Mechanism. Since S_1 has an average oxidation state of 3.5,[35] the formation of two Mn(II) following hydroquinone treatment corresponds to at least an S_{-1} state (i.e. two electrons more reduced than S_1). An S_{-1} state could contain two Mn(II) and two Mn(IV) for an average oxidation state of 3.0. This is the oxidation state most consistent with the XANES spectrum[35] and would be consistent with the reduction of one $Mn(III)_2(\mu\text{-}O)_2$ dimer to Mn(II). However, since hydroquinone is present in excess, we cannot rule out the formation of a more reduced state. An S_{-3} state would be most likely since hydroquinone is typically a two-electron reductant. This could result, for example, from reduction of a $Mn(IV)_2(\mu\text{-}O)_2$ dimer to Mn(II). There is as yet no evidence for a stable S_{-3} state. However, S_{-2} states can be formed with hydrazine[57,58] or hydroxylamine,[58] providing precedent for the formation of states reduced beyond S_{-1}.

Mei and Yocum have shown that NH_2OH and H_2Q act synergistically in their ability to inactivate the OEC.[67] This demonstrates that these reagents attack different sites within the OEC. Our structural results support this picture. The NH_2OH-reduced samples show only minor structural perturbations despite the fact that they are EDTA sensitive. The H_2Q-reduced samples, on the other hand, show major structural perturbations but are *not* EDTA sensitive.[67] We have previously concluded, based on edge fits, that little or no Mn(II) is produced by NH_2OH, while substantial Mn(II) is produced by H_2Q.[35] This is completely consistent with the lack of significant structural changes in the EXAFS after reversible NH_2OH reduction and the marked structural changes that accompany H_2Q reduction.

The existence of two different sites of reduction is surprising. How can electrons be directed to a particular Mn simply by changing the nature of the reductant? In the following, we suggest one mechanism (Scheme 2) that can account for these observations. Hydroquinone is a bulky, hydrophobic reductant. We envision H_2Q having access to only two Mn within the time frame of our experiment. The H_2Q-sensitive site is labeled site A in Scheme 2. The smaller, hydrophilic NH_2OH can reduce the OEC both at site A and at a different, EDTA-sensitive site labeled site B. Since NH_2OH has access to both sites but preferentially attacks site B first, we identify this site as the high potential site. With longer incubations or with higher concentrations, NH_2OH also reacts with site A (see Figures 8 and 9) producing unstable, super-reduced states. Incubation with H_2Q followed by treatment with NH_2OH gives an unstable species that rapidly loses Mn(II).[67] In Scheme 2, this is explained by reduction of both site A (by H_2Q) and site B (by NH_2OH).

If site A has a lower reduction potential than site B, reduction of site A by H_2Q should be followed by electron transfer from site A to site B. That is, the final reduction product should be the same for H_2Q reduction and NH_2OH reduction. However, if site A is unstable after reduction and undergoes a structural rearrangement, this rearrangement could prevent internal electron equilibration. Consistent with this, we observe a major structural rearrangement following H_2Q reduction. In addition to H_2Q, a variety of other bulky reductants can reduce the OEC.[108] In common with H_2Q, reduction by all of these species is inhibited by chloride.[108] In contrast, reduction by NH_2OH

Scheme 2

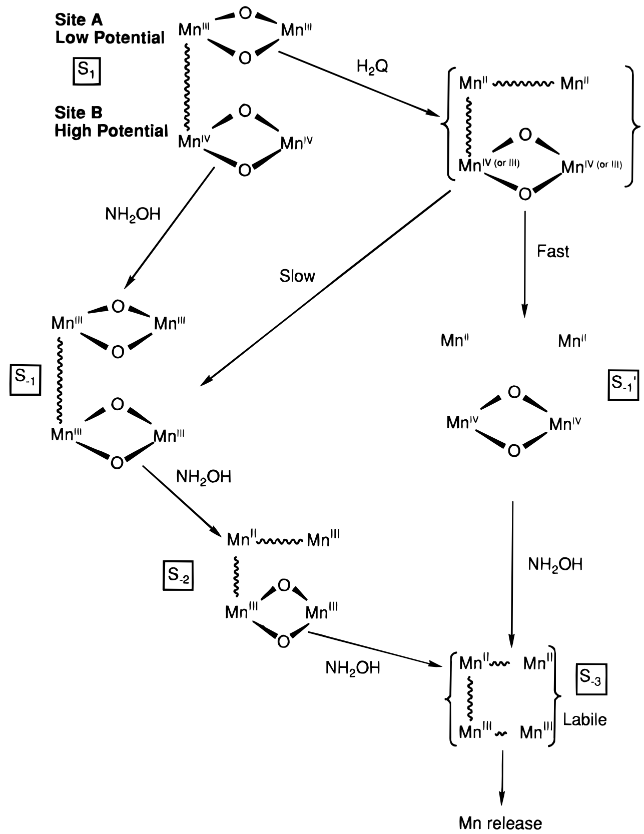

is not inhibited by chloride. In terms of Scheme 2, these results suggest that chloride inhibition blocks access to site A but not site B.

In addition to the schematic identification of sites A and B, Scheme 2 also includes a suggestion for the possible arrangement of atoms within these sites. The proposed structures are consistent with the observed EXAFS changes. However, given the uncertainties in the EXAFS, other assignments are clearly possible. In Scheme 2, site A is viewed as an oxo-bridged Mn(III) dimer. Two-electron reduction of this dimer would lead to an oxo-bridged Mn(II) dimer that would be expected to be unstable. This is consistent with the structural changes seen in the EXAFS and would explain the lack of internal electronic rearrangement if dimer decomposition is fast compared to internal electron transfer.

As noted above, the oxidation states (III,III),(III,III) are most consistent with the EXAFS for the NH_2OH produced S_{-1} state. The H_2Q-reduced species contains ca. 50% Mn(II) as determined by EPR and XANES. The remaining Mn could either be (IV,IV) or (III,III) depending on whether a two-electron or a four-electron reduction took place (i.e. "S_{-1}" or "S_{-3}"). We favor the S_{-1} assignment based on the stability of this state and because this assignment is most consistent with the XANES results.[35]

Relevance to Photoactivation. Photoactivation is the process in which the metal free OEC incorporates Ca^{2+}, Cl^-, and Mn^{2+} in the presence of light to form a fully active cluster. This process occurs with very low quantum yield (0.01)[70] and is highly dependent on the choice of electron acceptors and on the Ca^{2+} and Cl^- concentrations.[69,71,72,109] The prevailing model for photoactivation involves the initial incorporation of two tightly bound Mn. The photooxidation of the remaining two Mn is believed to be very efficient after the first pair has been

(108) Mei, R. Ph.D. Thesis, University of Michigan, 1993.

(109) Miyao, M.; Inoue, Y. *Biochemistry* **1991**, *30*, 5379−5387.

oxidized to Mn(III).[70−73] In photoactivation studies, the lowest oxidation state that is thought to be stable is a (II,II,III,III) tetramer.[72,73] In Scheme 2, this state corresponds to S_{-3}, which can be formed by NH_2OH but which, as shown in Figure 10, has limited stability. In the presence of light, S_{-3} oxidation competes with Mn(II) loss.[4] In the dark, however, S_{-3} is unstable due to the competing process of Mn(II) loss. In Scheme 2, site B is the most likely candidate for the site that is oxidized first in photoactivation. So long as this site is oxidized, as with the H_2Q-treated sample, the remaining Mn are stably sequestered, even though they may be present as Mn(II).

Conclusions

We have reported the structural characterization of two different reduced species of the Mn cluster of the OEC. In addition, we have provided spectroscopic evidence for states reduced beyond the S_{-1} state. We have shown that different reduced states are formed by H_2Q and NH_2OH reduction, based both on previously reported reactivity differences[67,68] and the structural differences reported here. One possible mechanism for these reductions is presented in Scheme 2. This scheme is consistent with the current understanding of the oxidation state of the Mn in S_1, with reduction schemes presented previously, and with the photoactivation process. In addition, EXAFS provides evidence for a structural rearrangement upon reduction that could prevent internal electron transfer between the different reduced species. Do the two "independent sites" identified in this study serve a mechanistic function? Perhaps the two sites exist because they catalyze two 2-electron oxidations.[110] In this model, one Mn site could catalyze the 2-electron oxidation of water to H_2O_2 while a second site could catalyze the 2-electron oxidation of H_2O_2 to O_2. A model containing dimers as the functional unit would be consistent with recent suggestions that a mixed valent dimer can account for the EPR properties of the OEC.[111] Regardless of the answer to this question, the existence of stable, distinct reduced states provides information about the possible configuration(s) of the Mn in the native cluster.

Acknowledgment. This research is supported in part by Grant No. USDA-NRICGP-92-37306-7662 to C.F.Y. and Grant No. GM-45205 from the US National Institute of Health to J.P.H. P.J.R.G. was supported in part by an NIH research traineeship. S.S.R.L. and N.S.L.S. are supported by the US Department of Energy with additional support from the NIH Research Resource program. We wish to thank Dr. Vincent Pecoraro, Dr. Nobumasa Kitajima, Dr. William Armstrong, and members of their respective research groups for helpful discussion and for supplying Mn model compounds that have aided in the interpretation of the protein data.

JA9504496

(110) Pecoraro, V. L. In *Manganese Redox Enzymes*; Pecoraro, V. L., Ed.; VCH Publishers: New York, 1992; pp 197−232.
(111) Åhrling, K. A.; Pace, R. J. *Biophys. J.* **1995**, *68*, 2081−2090.